Modeling strain-induced dual-phase transformation in semicrystalline polylactide

Hanen Mahjoubi, Fahmi Zaïri, Iurii Vozniak, Zoubeir Tourki, Fahed Zaïri

Mechanics of Time-Dependent Materials
https://doi.org/10.1007/s11043-022-09563-y

Modeling strain-induced dual-phase transformation in semicrystalline polylactide

Hanen Mahjoubi[1] · Fahmi Zaïri[2] · Iurii Vozniak[3] · Zoubeir Tourki[1] · Fahed Zaïri[4]

Received: 21 April 2022 / Accepted: 6 July 2022

Abstract
Polylactic acid or polylactide (PLA) can form amorphous, semicrystalline, or highly crystalline structure. In this paper, we provide a model for semicrystalline PLA under strain-induced dual-phase transformation, between mesomorphization and crystallization. In the proposed constitutive model, we use an internal state variable approach by considering initial microstructure, strain-induced dual-phase transformation, intermolecular features, and preferred network orientation-induced anisotropy. The effective contribution of the newly created phases is considered in both the elastic-viscoplastic intermolecular resistance and the viscohyperelastic network resistance using a micro–macro transition approach. We find a good agreement between the model and experimental data for the semicrystalline PLA in terms of progressive evolution of the mesomorphic/crystalline phases along with stress–strain behavior up to very large strains and over a wide range of crystallinities. The relationship between initial crystallinity, strain-induced molecular ordering, newly created phases, and mechanical response is discussed.

Keywords Semicrystalline polylactide · Strain-induced dual-phase transformation · Strain-induced chain orientation · Crystallinity effect · Elastic-viscoplastic-viscohyperelastic modeling

1 Introduction

Polylactide (PLA) is a very popular engineering environmental-friendly polymer derived from renewable agricultural resources and has a vast array of applications in the form of fibers, films, or massive parts. It is currently used for packaging (Auras et al. 2004; Armentano et al. 2013), but it is also a candidate for medical devices such as medical implants,

✉ F. Zaïri
fahmi.zairi@polytech-lille.fr

1 Sousse Mechanical Laboratory, Sousse University, 264 Sousse, Tunisia

2 Civil Engineering and geo-Environmental Laboratory (LGCgE), Lille University, 59000 Lille, France

3 Centre of Molecular and Macromolecular Studies, Polish Academy of Sciences, Sienkiewicza str., 112, Lodz 90363, Poland

4 Ramsay Générale de Santé, Hôpital privé Le Bois, 59000 Lille, France

Published online: 16 August 2022

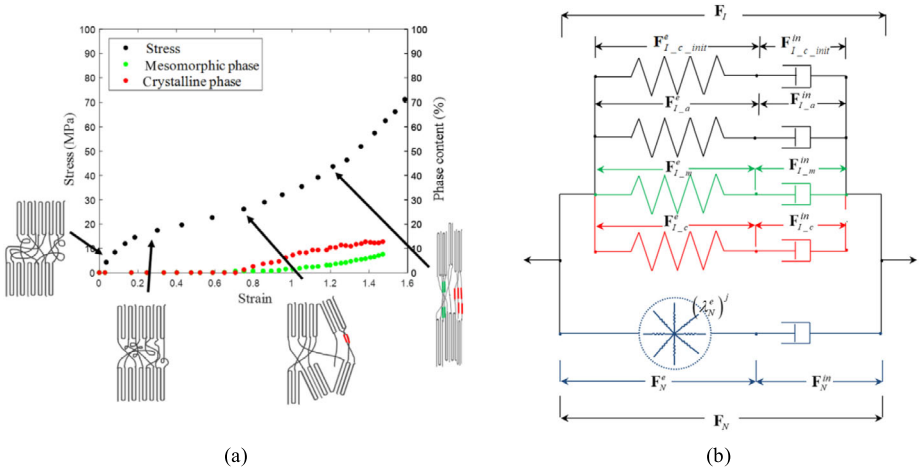

Fig. 1 Semicrystalline PLA mechanical response: (**a**) Typical tensile response including strain-induced dual-phase transformation established by Stoclet et al. (2012) by means of X-ray diffraction technique and (**b**) one-dimensional visualization of the model; the semicrystalline polymer resistance is split into an elastic-viscoplastic intermolecular resistance I constituted by four branches and a viscohyperelastic network resistance N

orthopedic devices, drug delivery systems, sutures in dermatology and cosmetics (Middleton and Tipton 2000; Agrawal and Bhalla 2003; Gupta et al. 2007; Vert 2015; Davachi and Kaffashi 2015; Li et al. 2020). Its biomedical applications originate from properties such as biocompatibility, bioresorbability, transparency, processability, and mechanical strength. Its mechanical properties are close to those of traditional petroleum-based polymers. Moreover, it is often used in 3D printing (Ligon et al. 2017; Gonzalez-Henriquez et al. 2019). An understanding of the PLA structure-property relationship is essential to provide accurate information for the PLA design.

The PLA can be amorphous or semicrystalline according to its stereochemical structure with a crystallinity degree up to 40% (Stoclet et al. 2012). PLAs containing more than 93% L-lactic acid are semicrystalline, whereas those containing between 50 and 93% L-lactic acid are completely amorphous (Tsuji and Ikada 1996). The semicrystalline PLA molecules have regular repeating units that allow the chains to fold into dense regions called crystallites, which reduce their flexibility and increase the intermolecular resistances. That results in higher glass transition and melting temperature compared with their amorphous counterpart. The level of crystallinity determines a large part of the mechanical, thermal, physical, chemical, and biodegradation properties. The crystallinity in PLA can come in different structures (α, β, and γ forms) depending on their preparation conditions (Pan and Inoue 2009). Crystallization from the molten state or from a solution leads to the formation of the most common α form (De Santis and Kovacs 1968; Miyata and Masuko 1997). Semicrystalline PLAs experience a phase transformation in the course of mechanical loading. Figure 1a provides an illustrative example of experimental results for a tensile test extracted from (Stoclet et al. 2012). The figure gives a general picture of the microstructural evolution during straining by considering as initial microstructure two crystalline lamellae separated by an amorphous phase. The plastic deformation of the crystalline lamellae is accompanied by the molecular ordering of the amorphous phase inducing a partial transformation into two newly formed substructures, an oriented crystalline form and an imperfect ordered mesomorphic form, possessing an intermediate ordering between amorphous and crystal. The

occurrence of the newly created phases strongly depends on the loading parameters in terms of strain rate and straining temperature (Picciochi et al. 2007; Delpouve et al. 2008; Stoclet et al. 2012).

Advanced engineering applications of semicrystalline PLA systems require tailoring and optimizing the microstructure evolution during deformation considering the complex competitive process of dual-phase changes with strong effects of loading parameters. That is a challenging task due to the complex multiscale relationship between macroresponse and microstructure in terms of initial molecular characteristics, initial ordered (crystalline) structures, degree of chain orientation, and phase transformation. In this regard, the development of quantitative predictive modeling of this relationship in semicrystalline PLA is a critical issue but has not been yet proposed in the literature. The strong influence of structural parameters (initial crystallinity and dual-phase transformation) and loading parameters (e.g., straining temperature) leads to versatile mechanical behaviors of the PLA from elastomeric type to thermoplastic type. Constitutive models for strain-induced phase transformation have been proposed within hyperelastic framework (Dargazany et al. 2014; Guo et al. 2018; Rastak and Linder 2018; Aygün and Klinge 2020; Guo and Zaïri 2020; Loos et al. 2021; Khiêm et al. 2022). The theoretical framework is suitable for the description of the strain-induced crystallization in crystallizable rubbers as a recoverable mechanism after complete unload of the sample. When strain-induced crystallization is an unrecoverable (thermomechanically stable) micromechanism and accompanied with plastic yielding, several constitutive models were proposed (Buckley and Jones 1995; Adams et al. 2000; Boyce et al. 2000; Rao and Rajagopal 2001; Ahzi et al. 2003; Makradi et al. 2005; Dupaix and Krishnan 2006; Shepherd et al. 2006; Dupaix and Boyce 2007; Regrain et al. 2009; Chevalier et al. 2012; Poluektov et al. 2013; Gehring et al. 2016; Mahjoubi et al. 2019, 2020). Apart from the papers of Mahjoubi et al. (2019, 2020), the previous models were restricted to petroleum-based polyethylene terephthalate. A unified elastic-viscoplastic-viscohyperelastic constitutive model was proposed by Mahjoubi et al. (2019, 2020) to capture the amorphous PLA time-temperature-dependent behavior along with strain-induced dual-phase transformation considering the competitive mesomorphization/crystallization occurrence with strong effects of loading parameters. The aim of the present work is adapting the latter for semicrystalline PLA to provide a model predicting the influence of the microstructural features (in terms of initial crystallinity, strain-induced molecular ordering, and newly created phases) on the overall mechanical response. The model capacities are verified by comparison of simulations and experimental observations on semicrystalline PLA containing a wide range of crystallinities and strained up to very large strains. The model is then used to highlight the influence of the initial crystallinity on the overall mechanical response evolution and the internal molecular ordering.

The outline of the paper is as follows. In Sect. 2, we provide the main features of the model formulation. In Sect. 3, we present the model application to semicrystalline PLA. Section 4 closes the paper with concluding remarks.

2 Model formulation

This section presents the main elements of the finite deformation elastic-viscoplastic-viscohyperelastic constitutive model.

We use the following notation. Tensors and vectors are denoted by normal boldfaced letters and italicized boldfaced letters, respectively, whereas scalars and individual components of vectors and tensors are denoted by normal italicized letters. The superposed dot

represents the time derivative. The prime denotes the deviatoric part. The superscript T denotes the transpose.

A rheological representation is schematically given in Fig. 1b. A brief description of the kinematics is provided in Appendix A. The superscripts e and in refer to the elastic and inelastic parts, respectively. The intermolecular interactions between neighboring polymer segments (referred with the subscript I), at the origin of the elastic-viscoplastic response at small/moderate strains, are introduced by parallel branches. Four separate branches, constituted by a linear elastic spring in series with a viscoplastic damper, are employed to consider the intermolecular barriers and flow increase due to the presence of crystals and the occurrence of dual phase. The subscripts a, c_init, m, and c refer to the amorphous, initial crystalline, and newly formed mesomorphic and crystalline phases, respectively. As a distinct deformation mechanism, a fifth branch is placed in parallel to represent the resistance to stretching/orientation and relaxation processes (referred with the subscript N) of the amorphous molecular chains network at the origin of the viscohyperelastic strain-hardening at large strains. The latter branch is represented by m hyperelastic springs in series with a nonlinear viscous damper. The m hyperelastic springs are introduced by means of the transition scale microsphere-based method to introduce the orientational effect.

2.1 Stress decomposition

The overall Cauchy stress tensor $\boldsymbol{\sigma}$ in the semicrystalline polymer is given by

$$\boldsymbol{\sigma} = \boldsymbol{\sigma}_I + \boldsymbol{\sigma}_N, \tag{1}$$

where $\boldsymbol{\sigma}_I$ is the intermolecular Cauchy stress tensor, and $\boldsymbol{\sigma}_N$ is the network Cauchy stress tensor.

The mechanical coupling between the four elementary deformation mechanisms in the intermolecular resistance I is obtained by the simple rule of mixture (Mahjoubi et al. 2019)

$$\boldsymbol{\sigma}_I = \left(1 - \chi_{c\_init} - \chi_m - \chi_c\right)\boldsymbol{\sigma}_{I\_a} + \chi_m \boldsymbol{\sigma}_{I\_m} + \chi_c \boldsymbol{\sigma}_{I\_c} + \chi_{c\_init}\boldsymbol{\sigma}_{I\_c\_init}, \tag{2}$$

where χ_{c_init} is the volume fraction of the initial crystalline phase, and, χ_m and χ_c are the volume fractions of newly formed (mesomorphic and crystalline) phases, for which the kinetics are governed by an Avrami-type expression specified in Sect. 2.3 (Eq. (11)).

From a Hencky strain energy function (logarithmic strain-based hyperelasticity law; see, e.g., Mirkhalaf et al. 2016) the intermolecular Cauchy stress tensor $\boldsymbol{\sigma}_{I\_i}$ in each phase i may be constitutively given by

$$\boldsymbol{\sigma}_{I\_i} = \frac{1}{J^e_{I\_i}} \mathbf{C}^e_{I\_i} \ln\left(\mathbf{V}^e_{I\_i}\right), \tag{3}$$

where $J^e_{I\_i}$ is the determinant of the elastic deformation gradient tensor $\mathbf{F}^e_{I\_i} = \mathbf{V}^e_{I\_i}\mathbf{R}^e_{I\_i}$ with stretching and rotation parts $\mathbf{V}^e_{I\_i}$ and $\mathbf{R}^e_{I\_i}$, and $\mathbf{C}^e_{I\_i}$ is the fourth-order isotropic elastic stiffness tensor expressed in Cartesian components using the Young modulus E_i and Poisson ratio ν_i as follows:

$$\left(\mathbf{C}^e_{I\_p}\right)_{ijkl} = \frac{E_p}{2\left(1+\nu_p\right)}\left[\left(\delta_{ik}\delta_{jl} + \delta_{il}\delta_{jk}\right) + \frac{2\nu_p}{1-2\nu_p}\delta_{ij}\delta_{kl}\right] \tag{4}$$

with δ_{ij} denoting the Kronecker delta symbol.

The behavior of the amorphous molecular chains is described using the transition scale microsphere-based method (Bazant and Oh 1986; Miehe et al. 2004; Göktepe and Miehe 2005). By this way the model takes into account the anisotropic effects caused by the molecular ordering during the strain-hardening at large strains. A summary of the microsphere-based method is provided in Appendix B. The overall network Cauchy stress tensor $\boldsymbol{\sigma}_N$ can be written in the principal coordinate system as follows (Mahjoubi et al. 2019):

$$\sigma_{N\_k} = C_r \sum_{j=1}^{m} \omega^j \sqrt{N_a} \mathcal{L}^{-1}\left(\frac{\left(\lambda_N^e\right)^j}{\sqrt{N_a}}\right) \frac{\partial \left(\lambda_N^e\right)^j}{\partial \lambda_k} \lambda_k - P, \qquad k = 1, 2, 3, \tag{5}$$

in which $\mathcal{L}^{-1}(x)$ is the inverse Langevin function given by the Padé approximant, $\mathcal{L}^{-1}(x) \approx x\left(3 - x^2\right)/\left(1 - x^2\right)$, P is an arbitrary scalar due to incompressibility and determined from the boundary conditions, $\left\{\left(\lambda_N^e\right)^j\right\}_{j=1,\ldots,m}$ are the microelastic stretches, and $\left\{\omega^j\right\}_{j=1,\ldots,m}$ are the weight factors. The term $C_r = nkT$ is the initial hardening modulus (with n the average chain density, k the Boltzmann constant, and T the absolute temperature), and the term N_a is the average number of amorphous segments in a single molecular chain.

2.2 Inelastic flow

The tensors $\mathbf{D}_{I\_i}^{in}$ and $\mathbf{D}_N^{in}$ defining the specificity of the intermolecular and network inelastic strain rates are defined by the following general flow rules:

$$\mathbf{D}_{I\_i}^{in} = \dot{\gamma}_{I\_i}^{in} \frac{\boldsymbol{\sigma}'_{I\_i}}{\sqrt{2}\left\|\boldsymbol{\sigma}_{I\_i}\right\|} \quad \text{and} \quad \mathbf{D}_N^{in} = \dot{\gamma}_N^{in} \frac{\boldsymbol{\sigma}'_N}{\sqrt{2}\left\|\boldsymbol{\sigma}_N\right\|}, \tag{6}$$

where $\left\|\boldsymbol{\sigma}_{I\_i}\right\| = \sqrt{\text{trace}\left(\boldsymbol{\sigma}'_{I\_i}\boldsymbol{\sigma}'^{T}_{I\_i}\right)/2}$ is the effective value of $\boldsymbol{\sigma}_{I\_i}$, $\left\|\boldsymbol{\sigma}_N\right\| = \sqrt{\text{trace}\left(\boldsymbol{\sigma}'_N\boldsymbol{\sigma}'^{T}_N\right)/2}$ is the effective value of $\boldsymbol{\sigma}_N$, $\boldsymbol{\sigma}'_{I\_i}$ is the deviatoric intermolecular stress, $\boldsymbol{\sigma}'_{I\_i}$ is the deviatoric network stress, $\dot{\gamma}_{I\_i}^{in}$ and $\dot{\gamma}_N^{in}$ are the inelastic shear strain rates given, respectively, by the Argon (1973) expression for the thermally activated process (Boyce et al. 2000) and the Bergstrom–Boyce (1998) expression for the thermal-induced relaxation process of the amorphous molecular chains network:

$$\dot{\gamma}_{I\_i}^{in} = \gamma_{0\_i} \exp\left(-\frac{\Delta G_i}{kT}\left(1 - \frac{\left\|\boldsymbol{\sigma}_{I\_i}\right\|}{s_i}\right)\right) \quad \text{and} \quad \dot{\gamma}_N^{in} = C\left|\lambda_N^{in} - 1\right|^{-1}\left\|\boldsymbol{\sigma}_N\right\|, \tag{7}$$

in which γ_{0_i} is the preexponential constant, ΔG_i is the activation energy barrier to molecular mobility, s_i is the shear strength, C is the chain relaxation parameter, and $\lambda_N^{in} = \sqrt{\text{trace}\left(\mathbf{F}_N^{in}\mathbf{F}_N^{inT}\right)/3}$ is the inelastic stretch on each molecular chain in the amorphous network, where $\mathbf{F}_N^{in}$ is the inelastic network deformation gradient tensor. Note that λ_N^{in} must be slightly higher than 1.0 at the beginning of the loading process to avoid singularity; the stability of the numerical algorithm is ensured by the addition of a perturbation coefficient equal to 0.01. Similar evolutions of the inelastic flow were used in the literature in the context of strain-induced crystallization of polymers exhibiting a yield event (see, e.g., Boyce et al. 2000; Ahzi et al. 2003; Makradi et al. 2005; Mahjoubi et al. 2019).

2.3 Network evolution

The effective contribution of the two newly created substructures is introduced in the network stress by considering the following evolution of the number of amorphous segments in a single molecular chain N_a (Mahjoubi et al. 2019):

$$N_a = N_{chain}\left(1 - \chi_{chain\_m} - \chi_{chain\_c}\right), \tag{8}$$

where $\chi_{chain\_m} \in [0, 1]$ is the degree of strain-induced mesomorphic segments, and $\chi_{chain\_c} \in [0, 1]$ is the degree of strain-induced crystalline segments:

$$\chi_{chain\_m} = \frac{N_m}{N_{chain}} \quad \text{and} \quad \chi_{chain\_c} = \frac{N_c}{N_{chain}}. \tag{9}$$

The term N_m is the number of mesomorphic segments, N_c is the number of crystalline segments, and $N_{chain} = N_c + N_m + N_a$ is the total number of segments per chain.

Due to the different chains orientations in the microsphere with respect to the applied straining, the transition scale method allows the nonuniform distribution of the micromechanisms at the chain scale. The following conditions on the stretch λ_{chain} of a single molecular chain are applied:

$$\chi_{chain\_m} = \begin{cases} 0, & 1 \le \lambda_{chain} < \lambda_{inc\_m}, \\ \chi_m, & \lambda_{chain} \ge \lambda_{inc\_m}, \end{cases} \quad \text{and} \quad \chi_{chain\_c} = \begin{cases} 0, & 1 \le \lambda_{chain} < \lambda_{inc\_c}, \\ \chi_c, & \lambda_{chain} \ge \lambda_{inc\_c}, \end{cases} \tag{10}$$

where λ_{inc_m} and λ_{inc_c} are the incubation stretches below which there is no phase transformation directly extracted from experimental data (see Appendix C).

The overall degrees of newly formed phases χ_m and χ_c are given by

$$\chi_m = \phi_{\infty\_m}\kappa_m \quad \text{and} \quad \chi_c = \phi_{\infty\_c}\kappa_c, \tag{11}$$

where ϕ_{∞_m} and ϕ_{∞_c} are the maximum phase degrees, and κ_m and κ_c are the total degrees of transformation given by the Avrami-type kinetics (Doufas et al. 2000) in which the strain rate effect is considered:

$$\begin{aligned} \dot{\kappa}_m &= \frac{\dot{\varepsilon}}{\dot{\varepsilon}_{ref}} \alpha K_{av\_m} \left(-\ln\left(1 - \kappa_m\right)\right)^{\frac{\alpha-1}{\alpha}} \left(1 - \kappa_m\right) \quad \text{and} \\ \dot{\kappa}_c &= \frac{\dot{\varepsilon}}{\dot{\varepsilon}_{ref}} \alpha K_{av\_c} \left(-\ln\left(1 - \kappa_c\right)\right)^{\frac{\alpha-1}{\alpha}} \left(1 - \kappa_c\right), \end{aligned} \tag{12}$$

where $\dot{\varepsilon}$ is the applied strain rate, $\dot{\varepsilon}_{ref}$ is the reference strain rate, α is the Avrami exponent, and, K_{av_m} and K_{av_c} are the phase transformation rates given by the empirical form defined as (Doufas et al. 2000)

$$K_{av\_m} = 1.47 \times 10^{-3} \left(\frac{4\pi N u_m}{3\phi_{\infty\_m}}\right)^{1/3} \exp\left(-\left(\frac{T - 141}{47.33}\right)^2\right) \qquad \left[\mathrm{s}^{-1}, T \text{ in } ^\circ\mathrm{C}\right], \tag{13}$$

$$K_{av\_c} = 1.47 \times 10^{-3} \left(\frac{4\pi N u_c}{3\phi_{\infty\_c}}\right)^{1/3} \exp\left(-\left(\frac{T - 141}{47.33}\right)^2\right) \qquad \left[\mathrm{s}^{-1}, T \text{ in } ^\circ\mathrm{C}\right], \tag{14}$$

where Nu_m and Nu_c represent the number densities of nuclei.

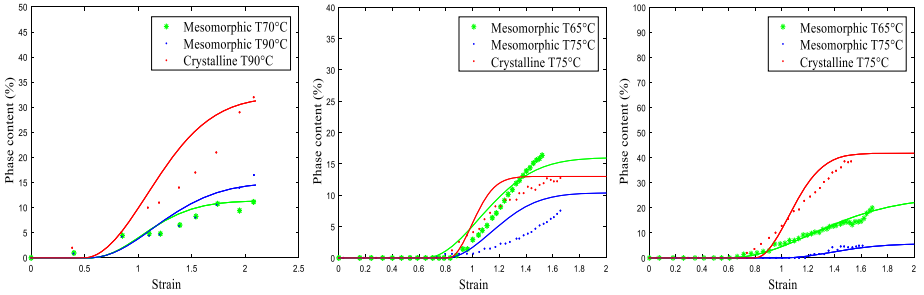

Fig. 2 Strain-induced phase transformation: (**a**) PLA40, (**b**) PLA24, and (**c**) PLA5 (symbols: experiments, lines: model)

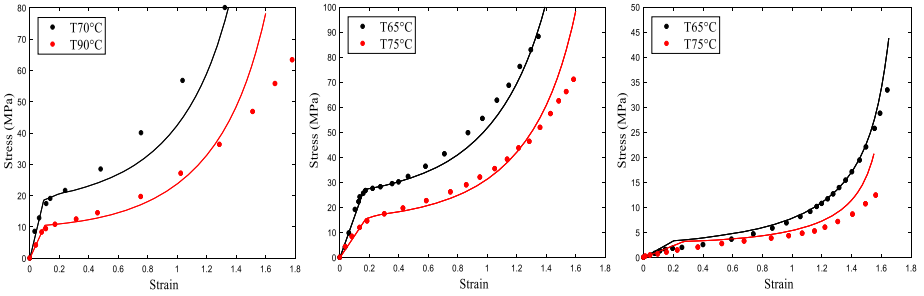

Fig. 3 Stress-strain response: (**a**) PLA40, (**b**) PLA24, and (**c**) PLA5 (symbols: experiments, lines: model)

3 Numerical results

The constitutive model was entirely coded in MATLAB software and is compared to the large tensile deformation behavior of three semicrystalline PLA systems containing 5%, 24%, and 40% crystal fractions.

3.1 Database

The three material systems will be denoted respectively as PLA5, PLA24, and PLA40. The experimental database extracted from the work of Stoclet et al. (2012) includes the following loading parameters:

$$\{\dot{\varepsilon} = 0.01/\mathrm{s},\ T = 65\ ^\circ\mathrm{C}\} \quad \text{and} \quad \{\dot{\varepsilon} = 0.01/\mathrm{s},\ T = 75\ ^\circ\mathrm{C}\} \quad \text{for PLA5}, \tag{15}$$

$$\{\dot{\varepsilon} = 0.01/\mathrm{s},\ T = 65\ ^\circ\mathrm{C}\} \quad \text{and} \quad \{\dot{\varepsilon} = 0.01/\mathrm{s},\ T = 75\ ^\circ\mathrm{C}\} \quad \text{for PLA24}, \tag{16}$$

$$\{\dot{\varepsilon} = 0.01/\mathrm{s},\ T = 70\ ^\circ\mathrm{C}\} \quad \text{and} \quad \{\dot{\varepsilon} = 0.01/\mathrm{s},\ T = 90\ ^\circ\mathrm{C}\} \quad \text{for PLA40}. \tag{17}$$

The experimental data are plotted, in the form of symbols, in Figs. 2 and 3 for the different loading parameters. The formation of newly formed phases follows a sigmoid kinetics strongly dependent on the initial amount of crystals. A small temperature variation results in significant changes in mesomorphic/crystalline phases occurrence along with in the material inelastic flow.

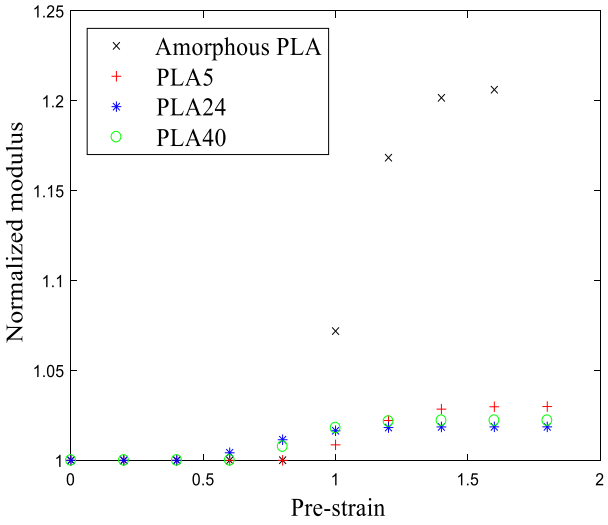

Fig. 4 Model results of the strain-induced stiffening in PLA

3.2 Model parameters

All the model parameters are provided in Appendix C. The kinetics of the strain-induced dual-phase transformation is firstly designed using the experimental data of Stoclet et al. (2012). Secondly, according to the model structure, the intermolecular parameters and the molecular network parameters are identified separately following a deterministic scheme. The intermolecular parameters both of the amorphous phase and of the newly formed phases are those already identified in a previous work by Mahjoubi et al. (2019) using the experimental database reported by Stoclet et al. (2010a, 2010b) of an initially amorphous PLA strained over a wide range of straining temperatures and two strain rates. All the other parameters were the outcome of a standard optimization procedure to extract the individual constitutive response of semicrystalline PLA using the experimental stress–strain curves of Stoclet et al. (2012).

3.3 Simulations vs. experiments

The simulation results are plotted in the form of solid lines in Figs. 2 and 3. The simulation consists in an isothermal straining under a constant strain rate of 0.01/s. The model is found to provide a good description of the strain-induced microstructure evolution over a wide range of crystallinities that are taken into account, with the strong and complex influence of straining temperature. The important features of the stress–strain behavior are also captured satisfactorily by the model over a large strain range including the initial elastic response, the yield event followed by the strain-hardening event. While considering the initial crystallinity, recall that the model considers the main physical processes occurring inside the material during the progressive strain-hardening response, namely the strain-induced chain orientation and anisotropy, the thermal-induced chain relaxation, and the micromechanisms of phase transformation.

3.4 Initial crystallinity effect

The role of the initial crystallinity on the strain-induced stiffening is presented in Fig. 4. The amorphous PLA stiffening obtained in a previous work by Mahjoubi et al. (2019) is also

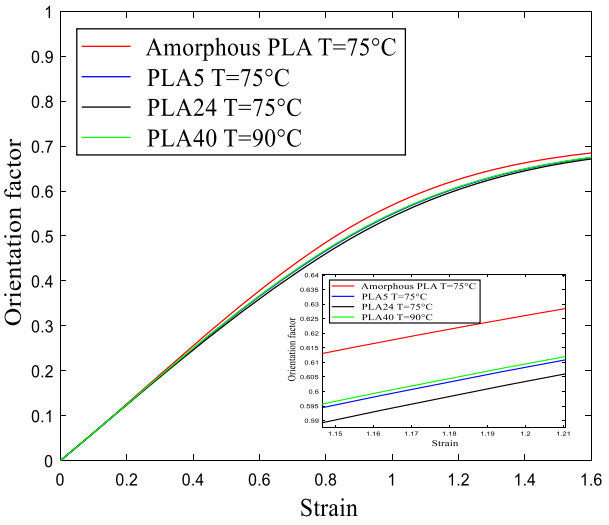

Fig. 5 Model results of the strain-induced molecular orientation in PLA

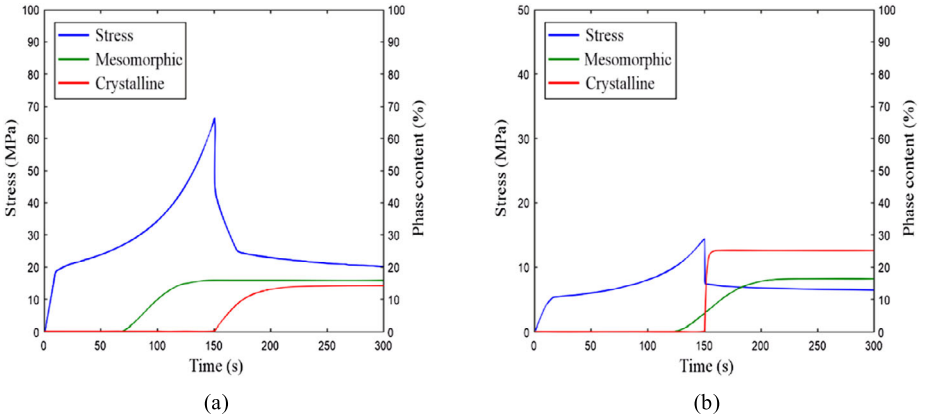

Fig. 6 Modeling results under continuous relaxation of (**a**) PLA24 and (**b**) PLA5 at a temperature of 65 °C followed by a heating until temperature of 75 °C

plotted in the figure. The results are presented for a loading condition leading to the solely development of the mesomorphic phase. As soon as the new phase appears, the PLA stiffness increases. Nonetheless, the stiffening in semicrystalline PLA is found significantly lower than that in amorphous PLA. As a key feature of our approach, the strain-induced internal molecular ordering and anisotropy were also predicted by the model and plotted in Fig. 5 using the orientation factor as indicator. The latter exhibits a linear evolution at small/moderate strains, and then a more gradual increase at larger strains follows. Whereas the increase in amount of ordered phases depends on the initial crystallinity, the strain-induced anisotropy effects caused by the molecular ordering are found rather quite insensible.

As a final point of discussion, the response during continuous relaxation combined with heating is analyzed in Fig. 6 for two initial crystallinities. The simulation consists of an isothermal straining at 65 °C up to a predetermined strain level of 1.5 under a constant strain rate of 0.01/s, and keeping this strain level constant for a prescribed delay during which

a progressive heating is performed at a constant rate until 75 °C. We can observe that the mesomorphic phase develops before relaxation for the two initial crystallinities, the strain-induced crystalline phase develops upon the temperature change during heating, whereas the mesomorphic phase remains unrecoverable. The stress evolution in response to heating combined with relaxation is significantly dependent on the initial crystallinity, whereas a strong connection is considered with the micromechanisms of phase transformation, chain orientation, and relaxation.

4 Concluding remarks

We have presented a physically based model able to capture the elastic-viscoplastic-viscohyperelastic behavior of semicrystalline PLA along with the mesomorphization/crystallization caused by the straining. The model considers the influence of the initial crystallinity on the competitive process of dual-phase transformation in relation to the strain-induced molecular ordering. A quantitative evaluation of the model was presented under uniaxial straining, and favorable comparisons to experimental observations were shown over a wide range of crystallinities. The model was then used to clarify the influence of the initial crystallinity on the strain-induced molecular ordering and the overall mechanical response.

The model provides a useful tool to better understand the separate and synergistic effects of key factors (microstructure features and loading parameters) governing the strengthen mechanisms in semicrystalline PLA under uniaxial straining. A complete verification of the model capabilities under more complex mechanical loading conditions remains nonetheless an important issue for further investigations. Although quite sophisticated, the model needs improvement for a fully realistic description of the micromechanisms of mesomorphization and crystallization through a thermodynamic reasoning; see, e.g., Guo and Zaïri (2020).

Appendix A: Kinematics

The key quantity of the kinematics is the deformation gradient tensor $\mathbf{F} = \partial \boldsymbol{x}/\partial \boldsymbol{X}$ mapping a material point from its initial position $\boldsymbol{X}$ to the current position $\boldsymbol{x}$. Parallelism of the five branches implies isodeformation (Fig. 1b), and thus the deformation gradient tensors are equal:

$$\mathbf{F}_{I\_a} = \mathbf{F}_{I\_c\_init} = \mathbf{F}_{I\_m} = \mathbf{F}_{I\_c} = \mathbf{F} \quad \text{and} \quad \mathbf{F}_N = \mathbf{F}. \tag{18}$$

The intermolecular and network deformation gradient tensors $\mathbf{F}_{I\_i}$ and $\mathbf{F}_N$ can be then further decomposed into elastic and inelastic contributions via multiplicative forms using the conceptual sequence of configurations proposed by Lee (1969):

$$\mathbf{F}_{I\_i} = \mathbf{F}^e_{I\_i}\mathbf{F}^{in}_{I\_i} \quad \text{and} \quad \mathbf{F}_N = \mathbf{F}^e_N\mathbf{F}^{in}_N. \tag{19}$$

The time derivative is $\dot{\mathbf{F}} = \mathbf{L}\mathbf{F}$, in which $\mathbf{L} = \partial \boldsymbol{v}/\partial \boldsymbol{x}$ is the spatial velocity gradient with $\boldsymbol{v} = \partial \boldsymbol{x}/\partial t$ additively split into elastic and inelastic parts,

$$\mathbf{L}_{I\_i} = \dot{\mathbf{F}}_{I\_i}\mathbf{F}^{-1}_{I\_i} = \mathbf{L}^e_{I\_i} + \mathbf{L}^{in}_{I\_i} \quad \text{and} \quad \mathbf{L}_N = \dot{\mathbf{F}}_N\mathbf{F}^{-1}_N = \mathbf{L}_N = \mathbf{L}^e_N + \mathbf{L}^{in}_N. \tag{20}$$

The inelastic velocity gradients $\mathbf{L}^{in}_{I\_i}$ and $\mathbf{L}^{in}_N$ are given by

$$\mathbf{L}^{in}_{I\_i} = \mathbf{F}^e_{I\_i}\dot{\mathbf{F}}^{in}_{I\_i}\mathbf{F}^{in^{-1}}_{I\_i}\mathbf{F}^{e^{-1}}_{I\_i} = \mathbf{D}^{in}_{I\_i} + \mathbf{W}^{in}_{I\_i} \quad \text{and} \quad \mathbf{L}^{in}_N = \mathbf{F}^e_N\dot{\mathbf{F}}^{in}_N\mathbf{F}^{in^{-1}}_N\mathbf{F}^{e^{-1}}_N = \mathbf{D}^{in}_N + \mathbf{W}^{in}_N, \tag{21}$$

where $\mathbf{D}^{in}_{I\_i}$ and $\mathbf{W}^{in}_{I\_i}$ are the symmetric (deformation rate) and skew symmetric (spin rate) parts, respectively:

$$\mathbf{D}^{in}_{I\_i} = \frac{1}{2}\left(\mathbf{L}^{in}_{I\_i} + \mathbf{L}^{in^T}_{I\_i}\right) \quad \text{and} \quad \mathbf{W}^{in}_{I\_i} = \frac{1}{2}\left(\mathbf{L}^{in}_{I\_i} - \mathbf{L}^{in^T}_{I\_i}\right). \tag{22}$$

Assuming irrotational inelastic flow both in the intermolecular resistance and the network resistance, the skew symmetric part of the inelastic velocity gradient vanishes, $\mathbf{W}^{in}_{I\_i} = \mathbf{0}$ and $\mathbf{W}^{in}_{N} = \mathbf{0}$, without loss in generality (Gurtin and Anand 2005), and the evolution equation of the inelastic deformation gradients, $\mathbf{F}^{in}_{I\_i}$ and $\mathbf{F}^{in}_{N}$, becomes

$$\dot{\mathbf{F}}^{in}_{I\_i} = \mathbf{F}^{e^{-1}}_{I\_i}\mathbf{D}^{in}_{I\_i}\mathbf{F}^{e}_{I\_i}\mathbf{F}^{in}_{I\_i} \quad \text{and} \quad \dot{\mathbf{F}}^{in}_{N} = \mathbf{F}^{e^{-1}}_{N}\mathbf{D}^{in}_{N}\mathbf{F}^{e}_{N}\mathbf{F}^{in}_{N}, \tag{23}$$

where the elastic deformation gradient tensors $\mathbf{F}^{e}_{I\_i}$ and $\mathbf{F}^{e}_{N}$ are then deduced from the deformation multiplicative decomposition (19).

Appendix B: Microsphere-based approach

The transition scale microsphere-based approach is employed to consider the orientational effect and the effect of the newly formed phase on the strain-hardening. In this approach a material point is represented by a unit sphere O_0 including a uniform distribution of m molecular chains, the chain end-to-end distance representing the microsphere radius (Miehe et al. 2004; Göktepe and Miehe 2005). The orientation of a molecular chain is parameterized by the classical spherical angles $\left\{\varphi^{j}_{chain}\right\}_{j=1,\ldots,m} \in [0, \pi]$ and $\left\{\theta^{j}_{chain}\right\}_{j=1,\ldots,m} \in [0, 2\pi]$. The average $\langle \upsilon \rangle$ of a microvariable υ is obtained by integration over the microsphere of total area $|\zeta|$:

$$\langle \upsilon \rangle = \frac{1}{|\zeta|}\int_{\zeta} \upsilon\left(\boldsymbol{r}_{chain}\right) dA, \tag{24}$$

where dA is the infinitesimal area of the unit sphere.

The continuous integration over the continuous space orientations is approximated by a discrete sum of a set of m orientations:

$$\langle \upsilon \rangle \approx \sum_{j=1}^{m} \upsilon\left(\boldsymbol{r}^{j}_{chain}\right)\omega^{j}. \tag{25}$$

A set of $m = 21$ integration points for a hemisphere is adopted as suggested by Bazant and Oh (1986) and Miehe et al. (2004). The weight factors $\left\{\omega^{j}\right\}_{j=1,\ldots,m}$ satisfy the following expression:

$$\sum_{j=1}^{m} \boldsymbol{r}^{j}_{chain}\omega^{j} = 0. \tag{26}$$

The terms $\left\{\boldsymbol{r}^{j}_{chain}\right\}_{j=1,\ldots,m}$ are the chain orientation unit vectors expressed in the Cartesian coordinate system by the following relation:

$$\boldsymbol{r}^{j}_{chain} = \boldsymbol{t}^{j}/\left|\boldsymbol{t}^{j}\right| = \cos\left(\theta^{j}_{chain}\right)\sin\left(\varphi^{j}_{chain}\right)\boldsymbol{x} + \sin\left(\theta^{j}_{chain}\right)\sin\left(\varphi^{j}_{chain}\right)\boldsymbol{y} + \cos\left(\varphi^{j}_{chain}\right)\boldsymbol{z}, \tag{27}$$

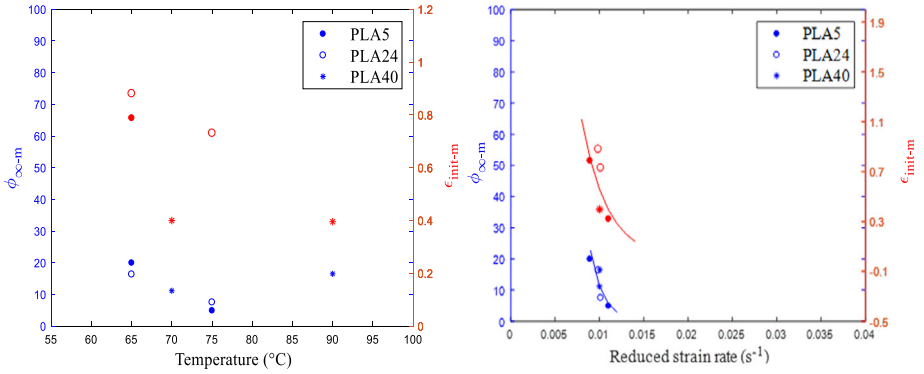

Fig. 7 Mesomorphic incubation strain and maximum phase degree as functions of (**a**) temperature and (**b**) reduced strain rate

where the term $\boldsymbol{t}^j = \mathbf{F}_N^e \boldsymbol{r}_{chain}^j$ is the deformed tangent with the elastic network deformation gradient tensor $\mathbf{F}_N^e$.

Accordingly, the azimuth angle $\left\{\varphi_{chain}^j\right\}_{j=1,\ldots,m}$ is expressed as

$$\varphi_{chain}^j = \cos^{-1}\left(t_3^j / \left|\boldsymbol{t}^j\right|\right) = \cos^{-1}\left(t_3^j / \left(\lambda_N^e\right)^j\right), \tag{28}$$

where $\left(\lambda_N^e\right)^j = \left|\boldsymbol{t}^j\right|$ is the microelastic stretch of a single molecular chain.

The criteria (10) of the main body of the paper allows the distribution of the two newly created phases on each molecular chain distributed uniformly in the microsphere. The incubation stretches are taken from the macroscopic observations (see Appendix C) and are directly used as constraints at the chain scale. The macrovariables of amounts are found by the averaging of all the molecular chains in the microsphere:

$$\langle \chi_m \rangle = \sum_{j=1}^{m} \chi_{chain\_m}^j \omega^j \quad \text{and} \quad \langle \chi_c \rangle = \sum_{j=1}^{m} \chi_{chain\_c}^j \omega^j, \tag{29}$$

where $\chi_{chain\_m}^j$ and $\chi_{chain\_c}^j$ are the microvariables obtained by projection on the orientation vector.

Appendix C: Parameters

C.1 Parameters of the dual-phase transformation

The number densities of nuclei Nu_m and Nu_c are expressed by the formulae

$$Nu_m = 2 \times 10^{10} \exp\left(-0.182T\right) \quad \text{and} \quad Nu_c = 3.2 \times 10^9 \exp\left(-0.111T\right) \quad [T \text{ in } ^\circ\text{C}]. \tag{30}$$

The incubation stretches λ_{inc_m} and λ_{inc_c}, from which the mechanism of phase transformation nucleates, and the maximum phase degrees ϕ_{∞_m} and ϕ_{∞_c} are directly taken from

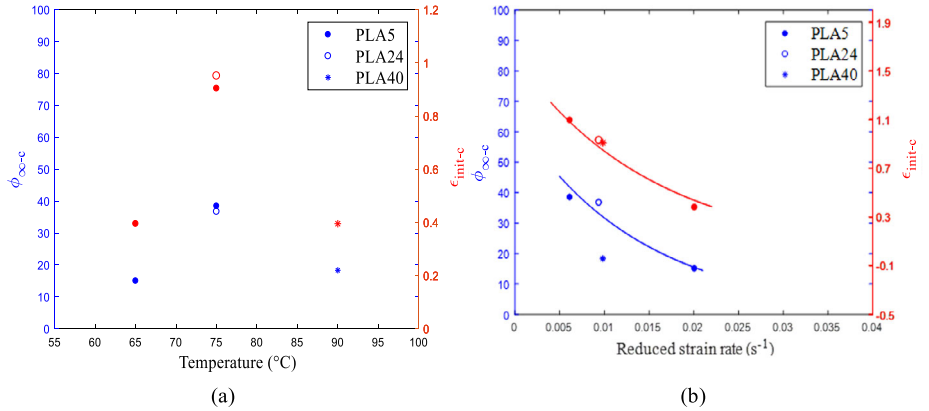

Fig. 8 Crystalline incubation strain and maximum phase degree as functions of (**a**) temperature and (**b**) reduced strain rate

Fig. 2 and reported in Figs. 7 and 8. The two quantities are significantly influenced by the straining temperature and the initial crystal fraction. It is possible to aggregate them by introducing the reduced strain rate, as observed in Figs. 7 and 8, and the following formulae can be used to describe them:

$$\lambda_{inc\_m} = 17.65 \exp\left(-345 a_{T\_m}\dot{\varepsilon}\right) \quad \text{and} \quad \lambda_{inc\_c} = 1.51 \exp\left(-65 a_{T\_c}\dot{\varepsilon}\right) \quad \left[\dot{\varepsilon} \text{ in s}^{-1}\right], \tag{31}$$

$$\phi_{\infty\_m} = 114.8 \exp\left(-692 a_{T\_m}\dot{\varepsilon}\right) \quad \text{and} \quad \phi_{\infty\_c} = 0.647 \exp\left(-71.4 a_{T\_c}\dot{\varepsilon}\right) \quad \left[\dot{\varepsilon} \text{ in s}^{-1}\right], \tag{32}$$

where $a_{T\_m}\dot{\varepsilon}$ and $a_{T\_c}\dot{\varepsilon}$ are the reduced strain rates for the mesophase and for the crystalline phase, respectively, expressed using the Williams–Landel–Ferry (so-called WLF) time-temperature equivalence principle

$$\ln\left(a_{T\_m}\right) = \frac{C_{1\_m}\left(T - T_{ref}\right)}{C_{2\_m} + T - T_{ref}} \quad \text{and} \quad \ln\left(a_{T\_c}\right) = \frac{C_{1\_c}\left(T - T_{ref}\right)}{C_{2\_c} + T - T_{ref}}, \tag{33}$$

where T_{ref} is the reference temperature taken equal to 70 °C, and C_{1_m}, C_{2_m}, C_{1_c}, and C_{2_c} are parameters adjusted to aggregate the data as much as possible. The following expressions as functions of the initial crystal fraction are found:

$$C_{1\_m} = 2\left(1 - \chi_m\right)^{10} \quad \text{and} \quad C_{2\_m} = 60\left(1 - \chi_m\right) \quad [°\text{C}], \tag{34}$$

$$C_{1\_c} = -5.47\left(1 - \chi_c\right)^{10} \quad \text{and} \quad C_{2\_c} = 30\left(1 - \chi_c\right) \quad [°\text{C}]. \tag{35}$$

C.2 Intermolecular parameters of the amorphous phase

The glassy-rubbery variation with temperature of the amorphous stiffness modulus E_a is described by the same formulae identified for the amorphous PLA in a previous work (Mahjoubi et al. 2019):

$$E_a = 402.85 - 2.273T \quad [\text{MPa}, T \text{ in } °\text{C}] \quad \text{for } T < T_g - \Delta T_g/2, \tag{36}$$

$$E_a = 128.92\left(1 - \tanh\left(\frac{5}{\Delta T_g}\left(T - T_g\right)\right)\right) - 0.783\left(T - T_g\right) \quad [\text{MPa},\ T \text{ in } ^\circ\text{C}] \quad \text{for } T \geq T_g - \Delta T_g/2, \tag{37}$$

where $\Delta T_g = 10\ ^\circ\text{C}$ is the glass transition interval.

The amorphous shear strength s_a and activation energy ΔG_a are those identified in a previous work (Mahjoubi et al. 2019):

$$s_a = 1.434 \times 10^4 \exp\left(-0.1307T\right) \quad [\text{MPa}, T \text{ in } ^\circ\text{C}] \quad \text{and} \quad \Delta G_a = 8 \times 10^{-19} \quad [\text{J}]. \tag{38}$$

The preexponential factor γ_{0_i} is taken identical for all the phases:

$$\gamma_{0\_a} = \gamma_{0\_c\_init} = \gamma_{0\_m} = \gamma_{0\_c} = 1.75 \times 10^6 \quad \left[\text{s}^{-1}\right]. \tag{39}$$

C.3 Intermolecular parameters of the initial crystalline phase

The initial crystalline stiffness modulus E_{c_init} is given by

$$E_{c\_init} = 54306 \exp\left(-0.07T\right) \quad [\text{MPa}, T \text{ in } ^\circ\text{C}] \quad \text{for PLA5 and PLA24,} \tag{40}$$

$$E_{c\_init} = 7.10^6 \exp\left(-0.14T\right) \quad [\text{MPa}, T \text{ in } ^\circ\text{C}] \quad \text{for PLA40.} \tag{41}$$

The shear strength s_{c_init} is given by

$$s_{c\_init} = 3634 \exp\left(-0.06T\right) \quad [\text{MPa}, T \text{ in } ^\circ\text{C}] \quad \text{for PLA5 and PLA24,} \tag{42}$$

$$s_{c\_init} = 160 \exp\left(-0.025T\right) \quad [\text{MPa}, T \text{ in } ^\circ\text{C}] \quad \text{for PLA40.} \tag{43}$$

The activation energy ΔG_{c_init} is given by

$$\Delta G_{c\_init} = 7 \times 10^{-19} \quad [\text{J}]. \tag{44}$$

C.4 Intermolecular parameters of the newly created phases

The values of the intermolecular parameters of the newly created phases are those identified in a previous work (Mahjoubi et al. 2019) for an initially amorphous PLA. The stiffness moduli of the created phases E_m and E_c are given by

$$E_m = 365688 \exp\left(-0.152T\right) \quad [\text{MPa}, T \text{ in } ^\circ\text{C}], \tag{45}$$

$$E_c = 12411 \exp\left(-0.077T\right) \quad [\text{MPa}, T \text{ in } ^\circ\text{C}]. \tag{46}$$

The mesomorphic shear strength s_m and activation energy ΔG_m are given by

$$s_m = 41918 \exp\left(-0.13T\right) \quad [\text{MPa}, T \text{ in } ^\circ\text{C}] \quad \text{and} \quad \Delta G_m = 7.5 \times 10^{-19} \quad [\text{J}]. \tag{47}$$

The values of s_c and ΔG_c for the newly formed crystalline phase are given by

$$s_c = 20095 \exp\left(-0.112T\right) \quad [\text{MPa}, T \text{ in } ^\circ\text{C}] \quad \text{and} \quad \Delta G_c = 7 \times 10^{-19} \quad [\text{J}]. \tag{48}$$

C.5 Network parameters

The average number of segments in a single molecular chain N_{chain} and the hardening modulus C_r are expressed as

$$N_{chain} = 3T - 140 \quad [T \text{ in } ^\circ\text{C}], \tag{49}$$

$$C_r = (-0.17T + 15.8)\, \chi_{c\_init} \quad [\text{MPa}, T \text{ in } ^\circ\text{C}] \quad \text{for PLA5 and PLA24}, \tag{50}$$

$$C_r = -0.02T + 2.50 \quad [\text{MPa}, T \text{ in } ^\circ\text{C}] \quad \text{for PLA40}. \tag{51}$$

The thermal-induced chain relaxation parameter C is given by

$$C = 4.10^{-8}T - 3.10^{-6} \quad \left[\text{MPa}^{-1}\,\text{s}^{-1}, T \text{ in } ^\circ\text{C}\right] \quad \text{for PLA5 and PLA24}, \tag{52}$$

$$C = 7.10^{-9}T - 2.10^{-7} \quad \left[\text{MPa}^{-1}\,\text{s}^{-1}, T \text{ in } ^\circ\text{C}\right] \quad \text{for PLA40}. \tag{53}$$

Data Availability The datasets generated during and/or analyzed during the current study are available from the corresponding author on reasonable request.

References

Adams, A.M., Buckley, C.P., Jones, D.P.: Biaxial hot drawing of poly(ethylene terephthalate): measurements and modelling of strain-stiffening. Polymer **41**, 771–786 (2000)

Agrawal, A.K., Bhalla, R.: Advances in the production of poly(lactic acid) fibers: a review. J. Macromol. Sci. **43**, 479–503 (2003)

Ahzi, S., Makradi, A., Gregory, R.V., Edie, D.D.: Modeling of deformation behavior and strain-induced crystallization in poly(ethylene terephthalate) above the glass transition temperature. Mech. Mater. **35**, 1139–1148 (2003)

Argon, A.S.: A theory for the low temperature plastic deformation of glassy polymers. Philos. Mag. **28**, 839–865 (1973)

Armentano, I., Bitinis, N., Fortunati, E., Mattioli, S., Rescignano, N., Verdejo, R., Lopez-Manchado, M.A., Kenny, J.M.: Multifunctional nanostructured PLA materials for packaging and tissue engineering. Prog. Polym. Sci. **38**, 1720–1747 (2013)

Auras, R., Harte, B., Selke, S.: An overview of polylactides as packaging materials. Macromol. Biosci. **4**, 835–864 (2004)

Aygün, S., Klinge, S.: Continuum mechanical modeling of strain-induced crystallization in polymers. Int. J. Solids Struct. **196–197**, 129–139 (2020)

Bazant, Z., Oh, B.: Efficient numerical-integration on the surface of a sphere. Z. Angew. Math. Mech. **66**, 37–49 (1986)

Bergstrom, J.S., Boyce, M.C.: Constitutive modeling of the large strain time-dependent behavior of elastomers. J. Mech. Phys. Solids **46**, 931–954 (1998)

Boyce, M.C., Socrate, S., Llana, P.G.: Constitutive model for the finite deformation stress-strain behavior of poly(ethylene terephthalate) above the glass transition. Polymer **41**, 2183–2201 (2000)

Buckley, C.P., Jones, D.C.: Glass-rubber constitutive model for amorphous polymers near the glass transition. Polymer **36**, 3301–3312 (1995)

Chevalier, L., Luo, Y.M., Monteiro, E., Menary, G.H.: On visco-elastic modelling of polyethylene terephthalate behaviour during multiaxial elongations slightly over the glass transition temperature. Mech. Mater. **52**, 103–116 (2012)

Dargazany, R., Khiêm, V.N., Poshtan, E.A., Itskov, M.: Constitutive modeling of strain-induced crystallization in filled rubbers. Phys. Rev. E **89**, 022604 (2014)

Davachi, S.M., Kaffashi, B.: Polylactic acid in medicine. Polym.-Plast. Technol. Eng. **54**, 944–967 (2015)

De Santis, P., Kovacs, A.J.: Molecular conformation of poly(S-lactic acid). Biopolymers **6**, 299–306 (1968)

Delpouve, N., Saiter, A., Mano, J.F., Dargent, E.: Cooperative rearranging region size in semi-crystalline poly(L-lactic acid). Polymer **49**, 3130–3135 (2008)

Doufas, A.K., McHugh, A.J., Miller, C.: Simulation of melt spinning including flow-induced crystallization Part I. Model development and predictions. J. Non-Newton. Fluid Mech. **92**, 27–66 (2000)

Dupaix, R.B., Boyce, M.C.: Constitutive modeling of the finite strain behavior of amorphous polymers in and above the glass transition. Mech. Mater. **39**, 39–52 (2007)

Dupaix, R.B., Krishnan, D.: A constitutive model for strain-induced crystallization in poly(ethylene terephthalate) (PET) during finite strain load-hold simulations. J. Eng. Mater. Technol. **128**, 28–33 (2006)

Gehring, F., Bouvard, J.L., Billon, N.: Modeling of time dependent mechanical behavior of polymers: comparison between amorphous and semicrystalline polyethylene terephthalate. J. Appl. Polym. Sci. **133**, 43837–43854 (2016)

Göktepe, S., Miehe, C.: A micro-macro approach to rubber-like materials. Part III: the micro-sphere model of anisotropic Mullins-type damage. J. Mech. Phys. Solids **53**, 2259–2283 (2005)

Gonzalez-Henriquez, C.M., Sarabia-Vallejos, M.A., Rodriguez-Hernandez, J.: Polymers for additive manufacturing and 4D-printing: materials, methodologies, and biomedical applications. Prog. Polym. Sci. **94**, 57–116 (2019)

Guo, Q., Zaïri, F.: A physically-based thermo-mechanical model for stretch-induced crystallizable rubbers: crystallization thermodynamics and chain-network crystallization anisotropy. Int. J. Plast. **131**, 102724 (2020)

Guo, Q., Zaïri, F., Guo, X.: Thermodynamics and mechanics of stretch-induced crystallization in rubbers. Phys. Rev. E **97**, 052501 (2018)

Gupta, B., Revagade, N., Hilborn, J.: Poly(lactic acid) fiber: an overview. Prog. Polym. Sci. **32**, 455–482 (2007)

Gurtin, M.E., Anand, L.: The decomposition F=Fe Fp, material symmetry, and plastic irrotationality for solids that are isotropic-viscoplastic or amorphous. Int. J. Plast. **21**, 1686–1719 (2005)

Khiêm, V.N., Le Cam, J.B., Charlès, S., Itskov, M.: Thermodynamics of strain-induced crystallization in filled natural rubber under uni- and biaxial loadings. Part II: physically-based constitutive theory. J. Mech. Phys. Solids **159**, 104712 (2022)

Lee, E.H.: Elastic-plastic deformation at finite strains. J. Appl. Mech. **36**, 1–6 (1969)

Li, C., Guo, C., Fitzpatrick, V., Ibrahim, A., Zwierstra, M.J., Hanna, P., Lechtig, A., Nazarian, A., Lin, S.J., Kaplan, D.L.: Design of biodegradable, implantable devices towards clinical translation. Nat. Rev. Mater. **5**, 61–81 (2020)

Ligon, S.C., Liska, R., Stampfl, J., Gurr, M., Mulhaupt, R.: Polymers for 3D printing and customized additive manufacturing. Chem. Rev. **117**, 10212–10290 (2017)

Loos, L., Aydogdu, A.B., Lion, A., Johlitz, M., Calipel, J.: Strain-induced crystallisation in natural rubber: a thermodynamically consistent model of the material behaviour using a serial connection of phases. Contin. Mech. Thermodyn. **33**, 1107–1140 (2021)

Mahjoubi, H., Zaïri, F., Tourki, Z.: A micro-macro constitutive model for strain-induced molecular ordering in biopolymers: application to polylactide over a wide range of temperatures. Int. J. Plast. **123**, 38–55 (2019)

Mahjoubi, H., Zaïri, F., Tourki, Z.: Strain-induced phase transformation in poly(lactic acid) across the glass transition: constitutive model and identification. Int. J. Non-Linear Mech. **118**, 103241 (2020)

Makradi, A., Ahzi, S., Gregory, R.V., Edie, D.D.: A two-phase self-consistent model for the deformation and phase transformation behavior of polymers above the glass transition temperature: application to PET. Int. J. Plast. **21**, 741–758 (2005)

Middleton, J.C., Tipton, A.J.: Synthetic biodegradable polymers as orthopedic devices. Biomaterials **21**, 2335–2346 (2000)

Miehe, C., Göktepe, S., Lulei, F.: A micro-macro approach to rubber-like materials. Part I: the non-affine micro-sphere model of rubber elasticity. J. Mech. Phys. Solids **52**, 2617–2660 (2004)

Mirkhalaf, S.M., Andrade Pires, F.M., Simoes, R.: An elasto-viscoplastic constitutive model for polymers at finite strains: formulation and computational aspects. Comput. Struct. **166**, 60–74 (2016)

Miyata, T., Masuko, T.: Morphology of poly(L-lactide) solution-grown crystals. Polymer **38**, 4003–4009 (1997)

Pan, P., Inoue, Y.: Polymorphism and isomorphism in biodegradable polyesters. Prog. Polym. Sci. **34**, 605–640 (2009)

Picciochi, R., Wang, Y., Alves, N.M., Mano, J.F.: Glass transition of semi-crystalline PLLA with different morphologies as studied by dynamic mechanical analysis. Colloid Polym. Sci. **285**, 575–580 (2007)

Poluektov, M., van Dommelen, J.A.W., Govaert, L.E., Yakimets, I., Geers, M.G.D.: Micromechanical modelling of short-term and long-term large-strain behaviour of polyethylene terephthalate. Model. Simul. Mater. Sci. Eng. **21**, 085015 (2013)

Rao, I.J., Rajagopal, K.R.: A study of strain-induced crystallization of polymers. Int. J. Solids Struct. **38**, 1149–1167 (2001)

Rastak, R., Linder, C.: A non-affine micro-macro approach to strain-crystallizing rubber-like materials. J. Mech. Phys. Solids **111**, 67–99 (2018)

Regrain, C., Laiarinandrasana, L., Toillon, S., Saï, K.: Multi-mechanism models for semi-crystalline polymer: constitutive relations and finite element implementation. Int. J. Plast. **25**, 1253–1279 (2009)

Shepherd, J.E., McDowell, D.L., Jacob, K.I.: Modeling morphology evolution and mechanical behavior during thermo-mechanical processing of semi-crystalline polymers. J. Mech. Phys. Solids **54**, 467–489 (2006)

Stoclet, G., Seguela, R., Lefebvre, J.M., Elkoun, S., Vanmansart, C.: Strain-induced molecular ordering in polylactide upon uniaxial stretching. Macromolecules **43**, 1488–1498 (2010a)

Stoclet, G., Seguela, R., Lefebvre, J.M., Rochas, C.: New insights on the strain-induced mesophase of poly(D,L-lactide): In situ WAXS and DSC study of the thermo-mechanical stability. Macromolecules **43**, 7228–7237 (2010b)

Stoclet, G., Seguela, R., Vanmansart, C., Rochas, C., Lefebvre, J.M.: WAXS study of the structural reorganization of semi-crystalline polylactide under tensile drawing. Polymer **53**, 519–528 (2012)

Tsuji, H., Ikada, Y.: Crystallization from the melt of poly(lactide)s with different optical purities and their blends. Macromol. Chem. Phys. **197**, 3483–3499 (1996)

Vert, M.: After soft tissues, bone, drug delivery and packaging, PLA aims at blood. Eur. Polym. J. **68**, 516–525 (2015)